

SEPARATE ADJUSTMENT OF TORQUE AND STIFFNESS FOR PNEUMATIC ROBOT ACTUATORS WITH ANTAGONISTIC ROTARY ELASTIC CHAMBERS

David Baiden*[~] Oleg Ivlev*[~]

* Friedrich-Wilhelm-Bessel-Institute (FWBI) Research Company, Germany

[~] Institute of Automation (IAT), University of Bremen, Germany

ABSTRACT

In modern applications robots share the workspace with humans for service tasks or they are even attached to the human body to provide assistance in movement training. A possible approach to realize “human-like” interaction is to adapt the robot compliance/stiffness appropriately, depending on the manipulation task and/or the capabilities of the individual person. This can for instance be accomplished with stiff actuators and evasive robot motions using force sensors (active compliance) or alternatively with inherent (passive) compliant actuators and an invariant position reference. With respect to safety, fluidic soft-actuators similar to pneumatic muscles are beneficial due to light-weight and adjustable passive compliance. However, even common position or force control for pneumatic muscles still remains challenging due to non-linear dependency on actuator displacement, air pressure as well as friction effects. This article presents an approach for separate torque and stiffness adjustment of direct acting soft-actuators with pneumatic *rotary elastic chambers* (REC) in antagonistic arrangement, which are usable for human-robot-interaction (HRI) applications.

Keywords: Pneumatic soft-actuators, antagonistic, stiffness, control

1 IMPORTANCE OF COMPLIANCE FOR HUMAN-ROBOT-INTERACTION

Robot application has expanded in recent years from conventional industrial pick and place scenarios to more safety critical tasks, where the demand is to operate in rehabilitation, service and medical surgery. In many applications physical contact between robot and human or even the attachment of a robotic exoskeleton to human limbs is intended. Therefore it is necessary to design robotic systems that exhibit compliant behaviour and are able to adapt to

human movement patterns. The development of safe and dependable robots especially suitable for HRI should consider at least three important aspects: i) mechanical design, ii) actuation principle and iii) control architecture.

The first mandatory step is to minimize the robot mass. In many respects a lightweight construction with reduced moving masses is beneficial. Besides the case of an impact with end-effector based robots, the wearer of an exoskeleton would have to carry the entire weight of the robot, if there are no means of gravity compensation. But mass reduction is limited, since it depends on torque requirements as for instance the payload of the robot.

The next step in the design process is to introduce compliance, i.e. spring-like behaviour into the actuation system. In contrast to a stiff actuator, a compliant drive will not remain at the specified position. It will rather allow position deviations which depend on the interaction forces, imitating a more natural human-like behaviour. Compliance for a stiff actuator can be implemented by means of feed-back control, using sensors to measure interaction forces.

Contact author: David Baiden^{1,2}

¹Friedrich-Wilhelm-Bessel-Institute (FWBI)
Research Company

²Institute of Automation (IAT), University of Bremen
Otto-Hahn-Allee, 28359 Bremen, Germany
Email: baiden@fwbi-bremen.de

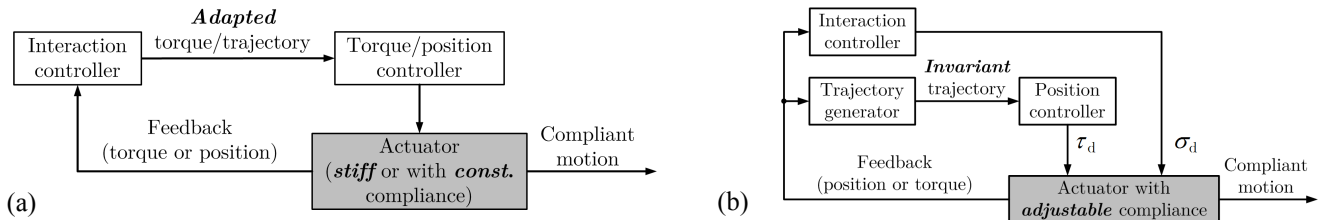


Figure 1 Realization examples to obtain compliant motion: (a) for stiff or constantly compliant actuators back-drivability and “human-like” interaction is imitated by torque or trajectory adaption; (b) with a fixed position reference the interaction controller creates back-drivability by direct actuator compliance adjustments.

This is denoted as *active compliance* and allows realizing back-drivability [1]. It is furthermore even possible to adjust compliance for the task requirement, but such an active system is not able to store energy and additional low controller bandwidth prevents to absorb high-frequency impacts. From this perspective the integration of a mechanical compliant element i.e. a spring, is specified as *passive compliance* and increases the safety level considerably.

It should be emphasised again, that inherent safety only results from naturally low impedance due to passive mechanical elements. However, the drawbacks are bandwidth restrictions that result in performance limitations. These relationships compel to compromise between safety and performance [2]. The desirable approach would be a combination between passive and active compliance, exploiting the benefits of inherent safety with adaptable compliance.

Control architecture is finally related to higher control layers, e.g. interaction controller and safety observer, whereas the latter is beyond the scope of this article. Interaction control should specify how a robot interacts with a human [3]. A frequently established fundament for “human-like” physical interaction control is based on impedance or stiffness (inverse of compliance) adaption [4]. With regard to the manipulation task and/or the capabilities of the individual person, the interaction controller should decide the level of adaption based on performance measures, which can be position errors or interaction forces [5, 6]. For *stiff* or *constantly compliant* actuators, this can be realized by evasive motions due to torque or trajectory adaption (Fig. 1 (a)). An alternative approach, which is followed here, is to use an invariant position reference and adjust the stiffness of the actuator, to allow position deviations (Fig. 1 (b)).

This paper presents an approach to independently adjust torque and stiffness of pneumatic soft-actuators with direct acting *rotary elastic chambers* (REC actuators) [7]. The purpose is to combine passive and active adjustable stiffness and integrate these modular soft-actuators into robots for safe physical HRI in orthopaedic and neurologic rehabilitation.

2 THE DIRECT ACTING ROTARY PNEUMATIC SOFT-ACTUATORS

The REC actuators are constructed of two fluid chambers in an antagonistic arrangement, similar to the principle of human muscles (Fig. 2). They are designed as direct acting rotary drives without gear and exhibit several distinctive properties like compactness and lightweight, paired with passive compliance [7]. Hydraulic or pneumatic operation is generally possible, if power supply and valve systems are appropriately adapted, such that oil, water or pressurized air is usable as fluid.

Air-pressured REC actuators convert pneumatic power into mechanical power and belong to the class of pneumatic muscles. If one chamber is inflated, i.e. the agonist, the internal air pressure increases and exerts a force to extend the chamber. The mechanical construction transfers this unidirectional expansion into a rotation and a torque is generated. In order to obtain turning into the opposite direction, the other chamber, i.e. the antagonist has to be charged. According to Fig. 2, the joint torque is the difference of the single chamber torques

$$\tau = \tau_2 - \tau_1. \quad (1)$$

Analysis and experiments in this paper are based on the patented pneumatic version, the *sREC* (DE 10 2011 081 727 A1) with skewed chambers (Fig. 3). However, control of this type of actuators is challenging due to non-linear behaviour and undesired effects like friction and hysteresis. For motion control two

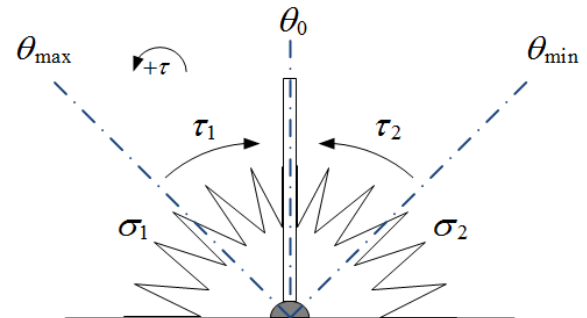


Figure 2 Working scheme of a fluidic soft-actuator with *rotary elastic chambers* (REC).



Figure 3 *sREC* actuator with skewed chambers (construction with unsymmetrical working range from 0 to approx. 45°).

valves and two pressure sensors are necessary to activate each chamber of a REC soft-actuator independently.

2.1 TORQUE MAP

In contrast to other approaches, where torque characteristics of actuators are mostly theoretically modelled with mathematical formulas based on physical relationships [8], the REC actuators are modelled experimentally. This procedure requires possessing plant and experimental setup in advance, but it is especially beneficial, if the internal structure of the system is unknown. Furthermore, quite precise models can be obtained with comparatively little effort in a short time.

The measurement routine is automated with a specifically developed test-rig shown in Fig. 4 [9]. Static torque values of one *single chamber* are captured in a specific sequence. Therefore an integrated electrical motor moves the actuator to predefined equally spaced angular positions across the whole operating range. At each position the pressure is varied with pressure proportional valves between 0–6 bar. The parameters are initial and final values of angle and pressure and in addition, angle and pressure resolutions $\delta\theta$ and δp , i.e. the step widths, are specified. The measurement starts according to Fig. 5 at the initial joint angle θ_1 with the initial pressure $p_{i,1}$, where each quantity can be either the minimum or maximum value and i indicates the number of the chamber. At the first position the pressure is stepwise incremented corresponding to $p_{i,k+1} = p_{i,k} + \delta p$ for $k = 1 \dots n$. Before commanding the motor to move the actuator to the next angle $\theta_{j+1} = \theta_j + \delta\theta$, the chamber is exhausted. Then the process is repeated for $j = 1 \dots m$, until the final angle is reached. Torque captures are only done in steady state, after



Figure 4 REC actuator mounted on the automated test-rig for torque characteristic measurements. The generated torque is measured at different angle-pressure combinations.

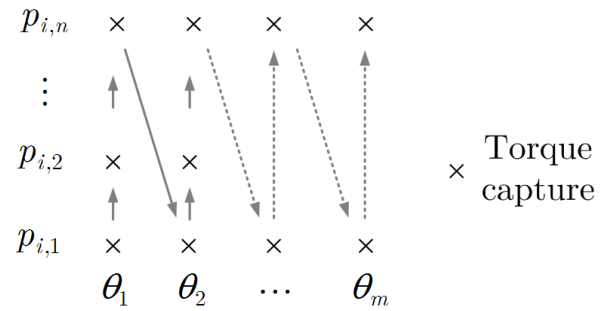


Figure 5 Sequence of static torque captures for one single chamber: the pressure is step-wise changed (increased or decreased) at a constant position. After venting, the actuator is placed to the next constant position where the process is repeated.

torque and pressure values remain within a selectable tolerance band for at least 5 sec. During this time span the motor brake is activated and the pressure proportional valve has attained the specified set point. Quite good results have been obtained with resolutions for pressure $\delta p = 1$ bar and angle $\delta\theta = 2.5^\circ$.

After data processing two static torque maps are obtained and stored in a look-up table. They reproduce the torque as non-linear function of pressure and angular position in form of

$$\tau_i = f(p_i, \theta) \tag{1}$$

where τ_i indicates the torque of one single chamber, p_i is the internal air pressure and θ is the joint angle.

Even though the opposite chamber is not actuated during measurement in the antagonistic setup, the stiffness influence of the material is still included. In order to account for friction effects, the average of two measurements with first increasing and then decreasing angle has been used.

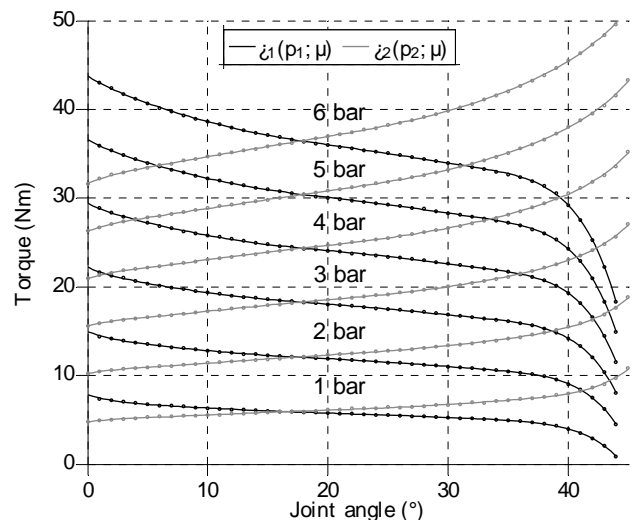


Figure 6 Averaged torque characteristic from two measurements with increasing and decreasing angle stored in data maps.

3 INDEPENDENT TORQUE AND STIFFNESS CONTROL

Stiffness control of actuators enables to adapt interaction forces of rehabilitation robots and is important with respect to human-like behaviour. In literature several approaches can be found, focusing mainly on position and stiffness control for linear pneumatic artificial muscles (PAM) or pneumatic cylinders. In this paper an approach for independent torque and stiffness adjustment of a rotary soft-actuator is presented, considering the individual torque characteristics of both pneumatic chambers.

3.1 EFFECTS OF THE DELTA-PRESSURE PRINCIPLE

In previous approaches that were mainly related to position control of the REC actuators, the motion control problem has been considered by applying the frequently used *delta-pressure* principle, as for example described in [10, 11]. This allows partitioning the single output of a position controller into two desired chamber pressures. Stiffness can be increased by adding the same offset pressure to both antagonistically arranged chambers, such that an additional torque is generated by each side

$$\begin{aligned} p_1 &= \Delta p + p_0 \\ p_2 &= -\Delta p + p_0 \end{aligned} \quad (2)$$

where p_1, p_2 are the resulting internal chamber pressures, Δp is the output of the position controller, i.e. a differential pressure and p_0 is the initial offset pressure. In this way the total pressure in each chamber is composed of one component, which should be solely responsible for motion (Δp) and another one, which only should have influence on stiffness (p_0), providing an adjustable compliant behaviour. With the choice $|\Delta p| \leq p_0 \leq p_s - |\Delta p|$, the resulting chamber pressures are limited to $0 \leq p_{(1,2)} \leq p_s$, where p_s is the supply pressure. Fig. 7 illustrates the simultaneous change of the two chamber pressures depending on the Δp -variable for several different constant offsets. The offset pressure should be selected, such that the adjustment ranges for the chamber pressures lay within usable bounds and both chambers participate simultaneously. In other words, a too low offset pressure value may lead to one-sided actuation by one chamber only, if a high controller output occurs. Likewise a too high value leads to desired values above the supply pressure. For equal internal pressures each chamber of a *symmetrically constructed* REC actuator only generates the same torque at the centre position, namely the natural equilibrium at θ_0 . Unequal chamber pressures, caused by arbitrary numbers of combinations between Δp and p_0 result in other torque balances at new equilibrium positions different from the natural equilibrium. The delta-pressure approach is appealing due to its simplicity, but there are several noteworthy limitations with respect to HRI control, as explained subsequently:

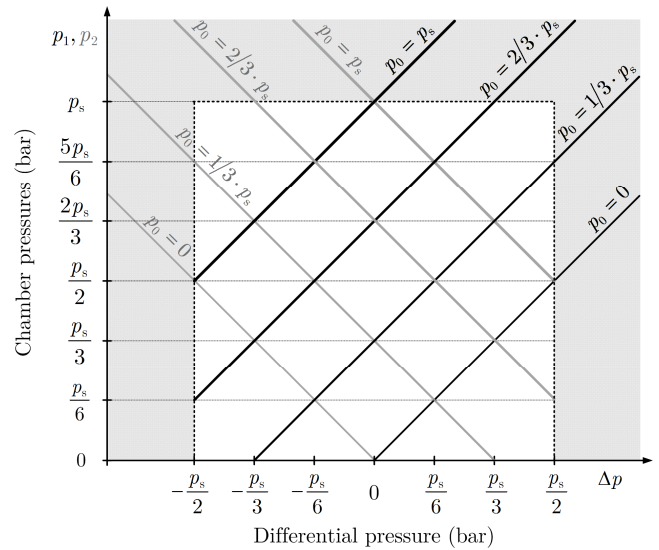


Figure 7 Resulting chamber pressures obtained by the delta-pressure principle with respect to the supply p_s .

- *Nominal value*: it is not possible to specify a particular nominal stiffness value in terms of the SI unit Nm/rad. The angle depending spring-like properties are not modelled and thus the resulting behaviour is not predictable.
- *Manual deflection*: another issue resulting from the same reason is recognizable by a manual deflection from any arbitrary equilibrium position, as indicated by Fig. 8. Assuming constant values for Δp and p_0 , a displacement, which is a linear change in angle, leads to a generation of non-linear restoring torques, meaning non-constant or *variable stiffness*.
- *Position deviation*: if at the natural equilibrium position the initial pressure p_0 and thus both chambers pressures are equally increased, the position remains constant. At any other equilibrium an increase of the p_0 -value promotes a deviation from the current position due to diverse single torques that do not compensate each other. Thus the actuator tends to move back to its natural equilibrium. This effect is not only relevant for open loop accuracy, but also affects a closed-loop position controller and requires *controller parameter adjustment* for any other p_0 -value.

Even though the delta-pressure principle enables to adjust compliance around a set point, adding a constant offset pressure for both chambers without incorporating the non-linear relation between pressure, angle and torque, revealed by the torque characteristic (Fig. 6) does not result in comprehensible defined spring-like properties. While the delta-pressure principle may be applicable in combination with a robust position controller, it cannot be utilized, when the inverted torque characteristics are applied for plant linearization and to enable torque control. The inverted relation directly dictates the total necessary chamber pressures

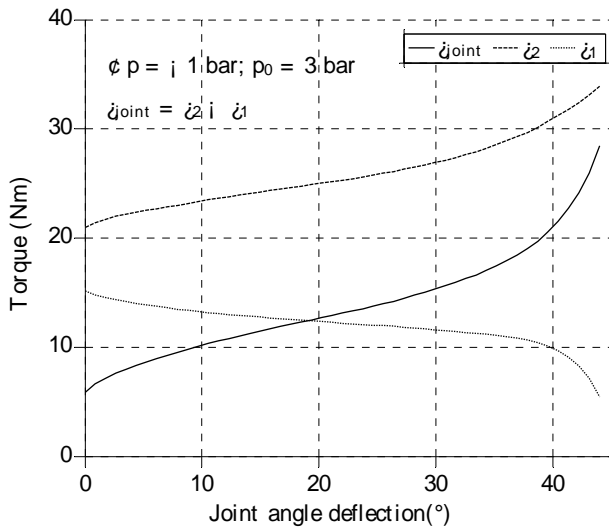


Figure 8 Manual deflection across the whole operating range at constant chamber pressures ($\Delta p = -1$ bar, $p_0 = 3$ bar): a linear change in angle leads to a generation of different non-linear restoring torques that do not compensate.

$$p_d = f^{-1}(\tau, \theta) = [p_{1d} \quad p_{2d}]^T \quad (3)$$

without any possibility to adjust the stiffness behaviour. Any additional offset pressure would distort the torque balance and subsequently cause a drift from the equilibrium position as well.

3.2 OTHER APPROACHES

Force and stiffness control for pneumatic cylinders has been demonstrated by Shen and Goldfarb [12] and similarly by Taheri *et al.* [13]. Due to sliding-mode controller design in the first case and back-stepping sliding-mode technique with valve dynamics incorporation in the latter case, impressive performance of the controllers was demonstrated with bandwidths of up to 4 Hz for sinusoidal torque and stiffness tracking. In [14] a sequential position and compliance control concept for enhanced safety of a 2 DOF pneumatic manipulator is presented. The actuator model is based on the commonly used representation by mass, spring and damping parameters. Because muscles are assumed to be identical, their angle dependency is expected to compensate. Ariga *et al.* implemented an equilibrium-point position and stiffness control for a set of antagonistic PAMs [15]. Two variables, representing the relation between the two muscle pressures and the difference of them respectively, allow adjusting position and stiffness intuitively. Due to the more linear PAM characteristics muscle forces are approximated linear with respect to contraction length and pressure. Another mechanical equilibrium model based on a geometrical approach is proposed by Nakamura *et al.* in order to compensate instantaneous load changes during position control [16]. Model and physical actuator show well correspondence, but the model establishment is quite sophisticated and furthermore torque feedback is required.

3.3 PARAMETRIC TORQUE CHARACTERISTIC

For torque-only model-based control, data maps can be utilized for plant linearization. However, in order to establish a linear relation between joint torque, joint stiffness and the two chamber pressures, neither the delta-pressure approach is suitable, nor data-based torque maps can be applied directly. Instead, parametric models are established that are identified based on the same measurement, which was initially used to create the torque maps. The parametric model for each torque characteristic can be approximated sufficiently accurate with linear pressure dependency and nonlinear angle dependency by an *individual polynomial* of type

$$\tau_i = \alpha_i(\theta)p_i + \beta_i(\theta) \quad (4)$$

where $i \in [1,2]$ indicates the chamber number. The term $\alpha_i(\theta)$ represents pressure and angle proportional constants, while $\beta_i(\theta)$ describes angle related coefficients only. They both describe the slopes and the intercepts of the approximated curves as polynomials

$$\alpha_i(\theta) = \sum_{j=0}^4 a_{ij}\theta^j \quad (5)$$

$$\beta_i(\theta) = \sum_{j=0}^5 b_{ij}\theta^j \quad (6)$$

where j is the index number. Substituting Eq. (5) and (6) into (4) results in the following expression

$$\begin{aligned} \tau_i = & b_{i5}\theta^5 + a_{i4}\theta^4 p_i + b_{i4}\theta^4 + a_{i3}\theta^3 p_i + b_{i3}\theta^3 \\ & + a_{i2}\theta^2 p_i + b_{i2}\theta^2 + a_{i1}\theta p_i + b_{i1}\theta \\ & + a_{i0} p_i + b_{i0} \end{aligned} \quad (7)$$

where the parameter b_{i0} can be understood as a global offset. By applying the least squares method, model parameters are estimated and fitted to the data sets of the torque maps. The obtained parametric torque characteristics of both chambers are plotted according to Fig. 9 for pressure values $p_i \in [1, 2, \dots, 6]$, revealing similar but not symmetrical trend.

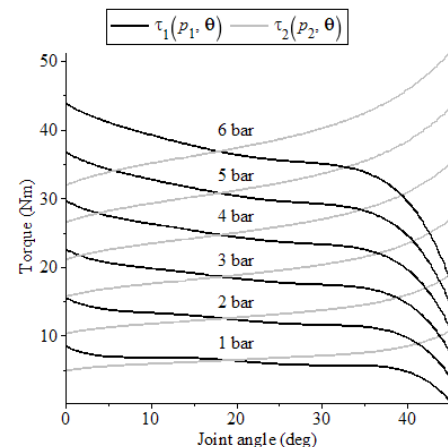


Figure 9 Approximated averaged torque characteristics of both chambers represented by individually fitted polynomials.

3.4 MODEL WITH INDEPENDENT TORQUE AND STIFFNESS INTERFACES

The parametric torque characteristics are used to model the joint torque, which is given by the difference of the single chamber torques

$$\begin{aligned}\tau &= \tau_2 - \tau_1 \\ &= \alpha_2(\theta) p_2 + \beta_2(\theta) - (\alpha_1(\theta) p_1 + \beta_1(\theta))\end{aligned}\quad (8)$$

while the joint stiffness is defined as the derivative of the joint torque with respect to the joint angle and must equal the sum of the single stiffness functions

$$\sigma = \frac{\partial \tau(p_2, p_1, \theta)}{\partial \theta} = \sigma_2 + \sigma_1 \quad (9)$$

where for $i \in [1, 2]$ each chamber stiffness is represented by

$$\begin{aligned}\sigma_i &= (4a_{i4}\theta^3 + 3a_{i3}\theta^2 + 2a_{i2}\theta + a_{i1})p_i \\ &\quad + (5b_{i5}\theta^4 + 4b_{i4}\theta^3 + 3b_{i3}\theta^2 + 2b_{i2}\theta + b_{i1}) \\ &= \Gamma_i(\theta) p_i + \Omega_i(\theta).\end{aligned}\quad (10)$$

For simplification Eqs. (7)–(10) are merged into a matrix equation

$$\begin{bmatrix} \tau \\ \sigma \end{bmatrix} = \mathbf{E} \begin{bmatrix} p_1 \\ p_2 \end{bmatrix} + \mathbf{r} \quad (11)$$

where

$$\begin{aligned}\mathbf{E}_{(2 \times 2)} &= \begin{bmatrix} -\alpha_1(\theta) & \alpha_2(\theta) \\ \Gamma_1(\theta) & \Gamma_2(\theta) \end{bmatrix}, \\ \mathbf{r}_{(2 \times 1)} &= \begin{bmatrix} \beta_2(\theta) - \beta_1(\theta) \\ \Omega_2(\theta) + \Omega_1(\theta) \end{bmatrix}\end{aligned}\quad (12)$$

for $\det(\mathbf{E}) \neq 0$, rearranging of Eq. (11) leads to

$$\begin{bmatrix} p_1 \\ p_2 \end{bmatrix} = \mathbf{E}^{-1} \left(\begin{bmatrix} \tau_d \\ \sigma_d \end{bmatrix} - \mathbf{r} \right). \quad (13)$$

The obtained system in Eq. (13) represents the REC actuator compliance model where the input values are desired torque τ_d and desired stiffness σ_d and the outputs are the two required pressure values. These are passed to the subsequent pressure controller as desired values $\mathbf{p}_d = [p_{1d} \ p_{2d}]^T$ according to Fig. 10, representing the implemented structure for real-time control. The pressure-valve subsystem is exchangeable for using either of-the-shelf pressure proportional valves or mass-flow proportional valves with specific pressure controllers that consider the dynamics of the pneumatic subsystem.

For the proposed approach it is important that the torque-pressure relationship is preferably linear with respect to pressure, such that the variable p can be incorporated into the polynomials with first order and thus Eq. (11) can easily be solved. Furthermore the order of the joint angle θ should be chosen relatively high, to preserve accuracy in the stiffness calculation after torque derivation.

3.5 SIMULATION ANALYSIS

Preceding simulation is conducted to investigate the expectable behaviour and understand the specific properties of the REC actuator. The modelled joint stiffness by Eq. (9) is plotted in Fig. 11 for several equal and distinctive pressure combinations in both chambers, revealing strong non-linearity. As mentioned before, each polynomial contains the influence of the opposite chamber. The quite stiff chamber material already provides a spring-like behaviour at zero pressure, therefore a minimum value 0.4 bar is required to compensate the *passive stiffness*. Due to the fact, that the pneumatic chambers cannot contract, it is only possible to control stiffness actively by varying pressure upwards, beginning from this level.

The next aspect of interest is the required pressure range. The graph in Fig. 12 contains both chamber pressures vs. joint angle for two contrasting examples a) low torque with high stiffness: $\tau_d = 1$ Nm, $\sigma_d = 0.4$ Nm/deg and conversely b) high torque with low stiffness $\tau_d = 15$ Nm, $\sigma_d = 0.2$ Nm/deg. Comparing again with Fig. 11, it is obvious that joint stiffness at the edges of the operating range is passively high and in these areas less pressure is necessary. By trend, for high stiffness values both pressures are increased, while for high torque values (either positive or negative) one pressure value is increased and the other one is reduced.

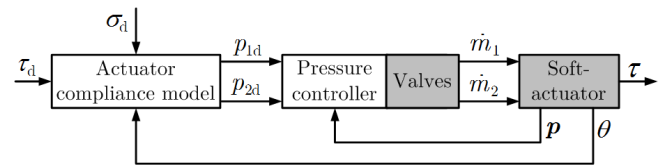


Figure 10 Control structure for independent torque and stiffness adjustment.

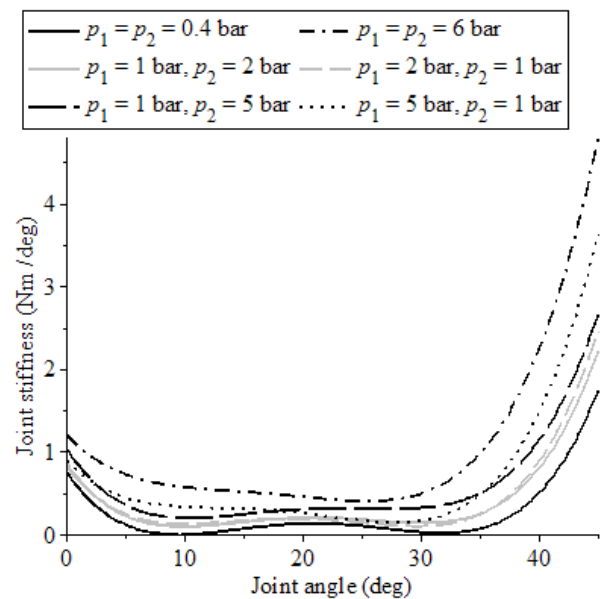


Figure 11 Simulated joint stiffness at different pressure combinations.

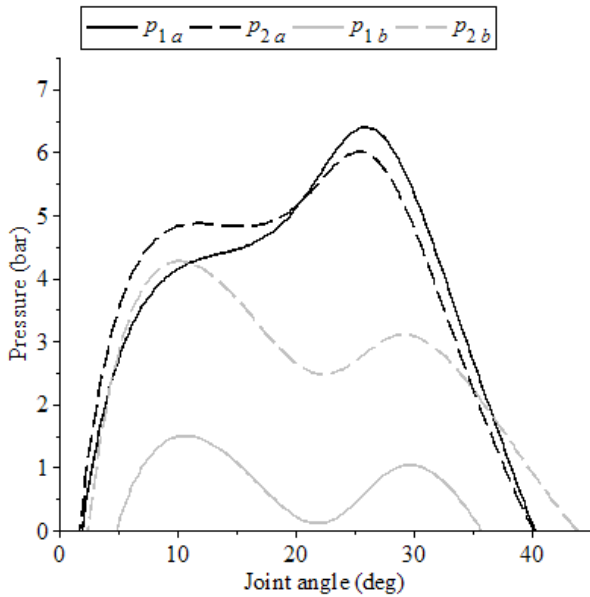


Figure 12 Simulation of required pressures for two example combinations of desired values: low torque with high stiffness (black lines) and high torque with low stiffness (grey lines).

In contrast to the previous torque-only control, the stiffness option reduces the maximal achievable joint torque. Based on these observations it can be concluded, that large torque commands lead to one-sided actuation which is in general similar to the torque-only approach, however with reduced accuracy. Furthermore because torque and stiffness are coupled by pressure, assuming a supply range between 0–6 bar, the desired values need to be chosen carefully in order to remain within valid pressure limits.

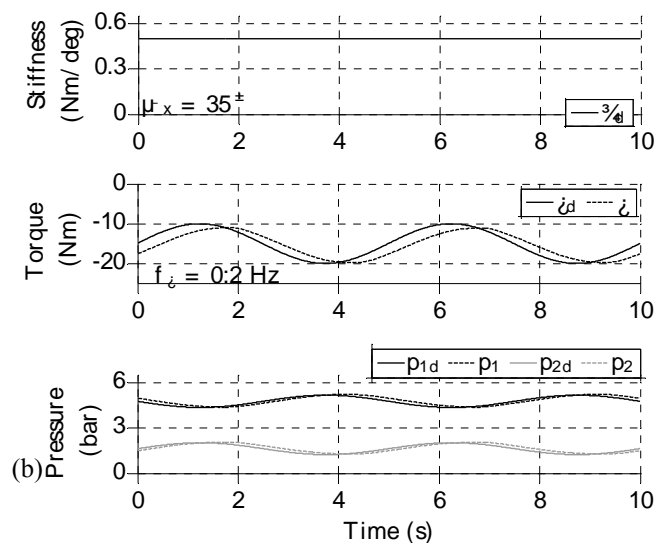
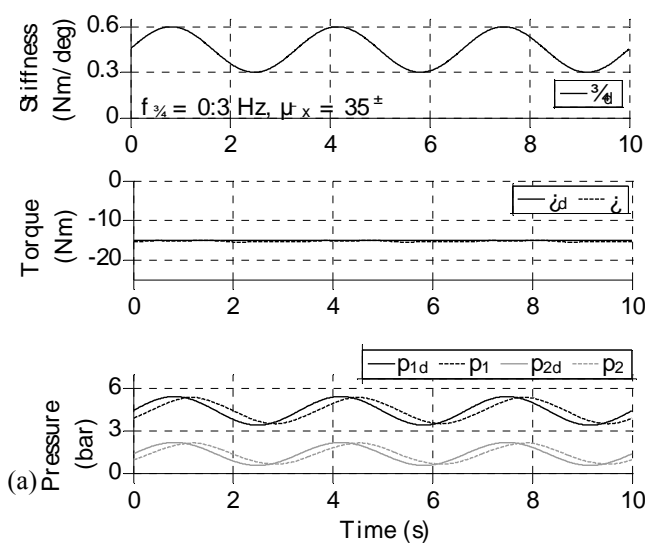


Figure 13 Experiments at constant position: (a) desired sinusoidal stiffness: $\sigma_d = 0.4 \pm 15$ Nm/deg, $f_\sigma = 0.3$ Hz and desired const. torque $\tau_d = -15$ Nm; (b) desired const. stiffness: $\sigma_d = 0.5$ Nm/deg and desired sinusoidal torque: $\tau_d = -15 \pm 5$ Nm, $f_\sigma = 0.2$ Hz.

4 EXPERIMENTAL RESULTS

The control structure according to Fig. 10 was implemented on a real-time signal processor board (*dSPACE, DS1102*) and model verification has been conducted by using the previously introduced test-rig (Fig. 4). For pressure control the integrated pressure proportional valves (*FESTO, VPPM-6L-L-1-G18-0L10H*) were utilized. The generated actuator torque and pressures were monitored with the integrated torque and pressure sensors (*HBM, TB1A* and *Sensortech, CTE 700 GU0*). Motor commanding and data capturing have been done manually. Three kinds of experiments have been carried out to illustrate the controller reaction during steady position, for unbounded conditions and furthermore to involve external interaction. To exclude gravity effects the actuator was horizontally orientated.

4.1 TORQUE AND STIFFNESS TRACKING AT CONSTANT POSITION

In the initial series of experiments the actuator was connected to the lever of the test-rig to fix it at any arbitrary constant position. At joint angle $\theta = 35^\circ$, first a constant desired torque $\tau_d = -15$ Nm in combination with a sinusoidal stiffness $\sigma_d = 0.4 \pm 15$ Nm/deg at frequency $f_\sigma = 0.3$ Hz was adjusted (Fig. 13 (a)). Despite pressure variation of $p_1 = 4.45 \pm 0.95$ bar and $p_2 = 1.4 \pm 0.8$ bar respectively, torque could be maintained nearly constant. Due to torque control, stiffness could not be measured directly by deflection experiments, but stiffness changes are noticeable in concurrent pressure adaption. Next, at the same angular position the shapes of the input trajectories were changed to sinusoidal torque $\tau_d = -15 \pm 5$ Nm, $f_\sigma = 0.2$ Hz and constant stiffness $\sigma_d = 0.5$ Nm/deg. Fig. 13 (b) shows that despite

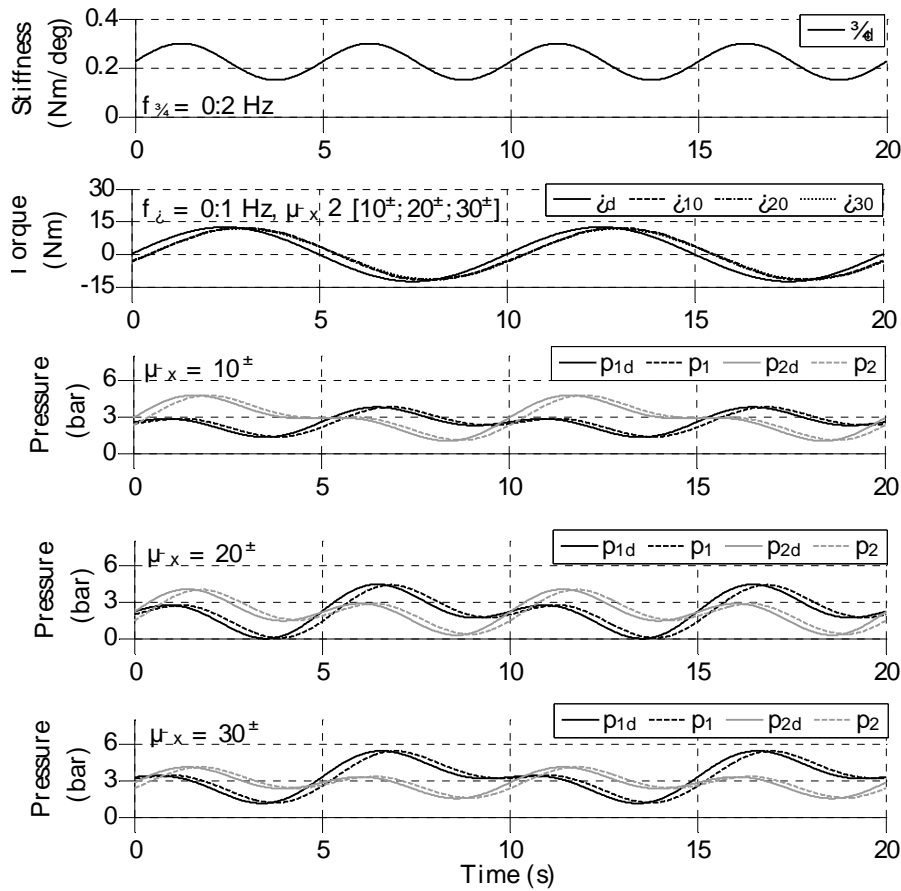


Figure 14 Superposition of desired sinusoidal torque and stiffness profiles at three different fixed angles.

smaller pressure variations $p_1 = 4.75 \pm 0.45$ bar and $p_2 = 1.65 \pm 0.35$ bar, torque is tracked with delay. Finally desired values for torque and stiffness have been set simultaneously with $f_{\sigma} = 0.2$ Hz and $f_{\tau} = 0.1$ Hz at $\theta_{fix} = \in [10^\circ, 20^\circ, 30^\circ]$ confirming the concept with similar results (Fig. 14).

4.2 STIFFNESS TRACKING UNDER UNCONSTRAINED CONDITION

In this experimental setup the actuator was detached from the motor to be unrestricted and the joint angle was measured with the actuator's integrated magnetic sensor (AMS, PRAS 21). Since torque is not measurable in this test, the desired torque was set to zero while stiffness was stepwise increased by $\Delta\sigma_d = 0.05$ Nm/deg and the focus was put on pressure and position deviations. Ideally the actuator should find its natural equilibrium and remain at this position for every adjusted stiffness value. As expected, both chamber pressures were simultaneously increased in accord with stiffness commands (Fig. 15), but this trial also exposed deficiencies in pressure control. Small position deviations of $\Delta\theta = \pm 1.8^\circ$ could be observed that are attribute to model inaccuracies.

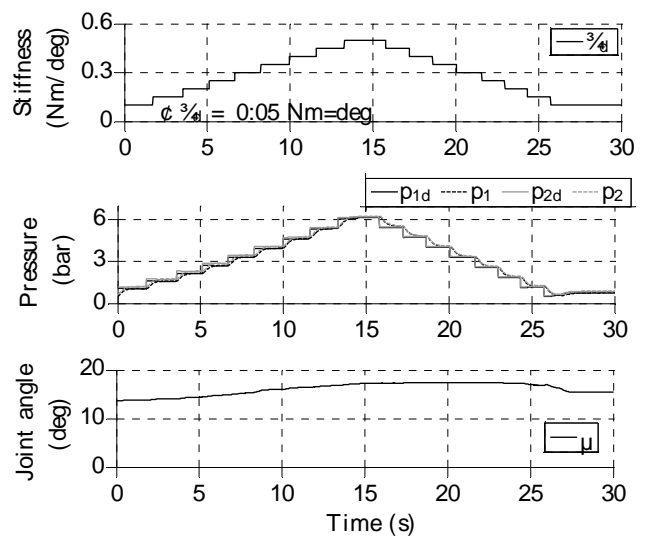


Figure 15 Step-wise change of desired stiffness with $\Delta\sigma_d = 0.05$ Nm/deg.

4.3 EMULATED HUMAN-ROBOT-INTERACTION

For the intended application in rehabilitation devices with physical contact to persons and adaptable HRI, the control response to external influences under dynamic conditions should be investigated. Therefore the REC was attached to the test-rig lever again and deflected by the motor in the sequence $\theta_d = 5-35-5^\circ$ with an angular velocity of $\dot{\theta}_d = 2 \text{ deg/s}$. The desired torque was set to $\tau_d = 5 \text{ Nm}$, while the desired stiffness was specified to $\sigma_d = 0.15 \text{ Nm/deg}$. Pressure values were tracked well in this test, however the maximal torque error of $\Delta\tau = 2 \text{ Nm}$ seems to be subject to uncompensated hysteresis effects due to the use of averaged torque characteristics.

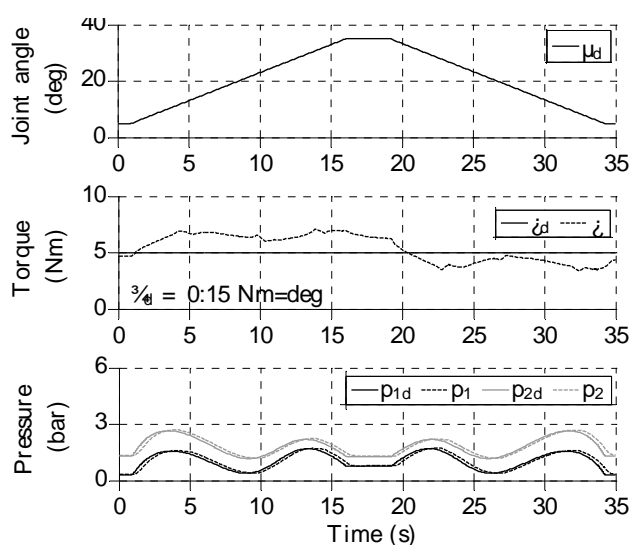


Figure 16 Torque and stiffness control under dynamic conditions with $\tau_d = 5 \text{ Nm}$, $\sigma_d = 0.15 \text{ Nm/deg}$, position sequence $\theta_d = 5-35-5^\circ$ and angular velocity $\dot{\theta}_d = 2 \text{ deg/s}$.

5 CONCLUSION AND FUTURE WORKS

First the importance of compliant actuation was discussed and rationales to develop pneumatic actuators with adjustable stiffness were exposed. Furthermore the limitations of the frequently applied delta-pressure principle have been explained in this paper.

Beginning from an experimental data-based model of the pneumatic REC actuators, torque and stiffness relationships have been derived and approximated by polynomials. The new model offers independent torque and stiffness interfaces for subsequent higher control layers, e.g. human-robot-interaction controllers. An explicit torque input might be advantageous, if the robot controller is based on torque control, which also enables to compensate for inaccuracies in a kinematic robot chain, especially when compensation of robot gravity is incorporated.

The presented model is able to cope with high torque-angle non-linearity and is basically applicable to all types of pneumatic muscles. Torque tracking performance could certainly be improved by utilizing mass flow proportional valves and applying the same model-based pressure con-

troller considering pressure dynamics, as already done in parallel ongoing research work. The approach requires the torque characteristic to be preferably linear with respect to pressure, in order to solve the approximated polynomials easily. Thus it is worthwhile to consider this aspect in future actuator chamber design. Similar to the previous torque-only control, there is neither torque nor stiffness feedback in the open loop structure. The choice of desired torque and stiffness combinations must be valid for keeping necessary pressure values within limited ranges. This is subject for future work as well as torque-angle hysteresis compensation.

6 ACKNOWLEDGEMENTS

This work was developed under the grant 13EZ1121A within the joint research project KoBSAR-II, supported by the German Federal Ministry of Education and Research (BMBF).

REFERENCES

- [1] Zinn M., Roth B., Khatib O., and Salisbury J. K., A new actuation approach for human friendly robot design. *The international journal of robotics research*, vol. 23, no. 4–5, pp. 379–398, 2004.
- [2] Bicchi A. and Tonietti G., Fast and "soft-arm" tactics [robot arm design]. *Robotics Automation Magazine, IEEE*, vol. 11, no. 2, pp. 22–33, June 2004.
- [3] Marchal-Crespo L. and Reinkensmeyer D. J., Review of control strategies for robotic movement training after neurologic injury. *Journal of neuroengineering and rehabilitation*, 6(1), 20, 2009.
- [4] Reinkensmeyer D. J., Kahn L. E., Averbuch M., McKenna-Cole A., Schmit B. D. and Rymer W. Z., Understanding and treating arm movement impairment after chronic brain injury: progress with the ARM guide. *Journal of rehabilitation research and development*, 37(6), pp. 653–662, 2000.
- [5] Krebs H. I., Palazzolo J. J., Dipietro L., Ferraro M., Krol J., Rankelev K., Volpe B. T. and Hogan N., Rehabilitation robotics: Performance-based progressive robot-assisted therapy. *Autonomous Robots*, 15(1), pp. 7–20, 2003.
- [6] Riener R., Lunenburger L., Jezernik S., Anderschitz, M. Colombo G. and Dietz V., Patient-cooperative strategies for robot-aided treadmill training: first experimental results. *Neural Systems and Rehabilitation Engineering, IEEE Transactions on*, 13(3), pp. 380–394, 2005.
- [7] Ivlev O., Soft fluidic actuators of rotary type for safe physical human-machine interaction. In *Rehabilitation Robotics, 2009. ICORR 2009. IEEE International Conference on*, pp. 1–5, June 2009.
- [8] Kelasidi E., Andrikopoulos G., Nikolakopoulos G., and Manesis S., A survey on pneumatic muscle actua-

- tors modelling. In *Industrial Electronics (ISIE), 2011 IEEE International Symposium on*, pp. 1263–1269, June 2011.
- [9] Rehr J. and Ivlev O., Automated torque testing machine for fluidic rotary soft-actuators. *tm-Technisches Messen*, vol. 78, no. 10, pp. 431–438, 2011.
- [10] Daerden F., Lefeber D., Verrelst B. and Van Ham R., Pleated pneumatic artificial muscles: actuators for automation and robotics. In *Advanced Intelligent Mechatronics, 2001. Proceedings. 2001 IEEE/ASME International Conference on (Vol. 2, pp. 738–743)*. IEEE.
- [11] Tsagarakis, N. G. and Caldwell, D. G., Development and control of a ‘soft-actuated’ exoskeleton for use in physiotherapy and training. *Autonomous Robots*, 15(1), pp. 21–33, 2003.
- [12] Shen X. and Goldfarb M., Simultaneous force and stiffness control of a pneumatic actuator. *Journal of Dynamic Systems Measurement and Control-Transactions of The Asme*, vol. 129, no. 4, pp. 425–434, 2007.
- [13] Taheri B., Case D., and Richer E., Design of robust nonlinear force and stiffness controller for pneumatic actuators. In *Decision and Control (CDC), 2012 IEEE 51st Annual Conference on*, pp. 1192–1198, Dec 2012.
- [14] Choi T.-Y., Choi B.-S., and Seo K.-H., Position and compliance control of a pneumatic muscle actuated manipulator for enhanced safety. *Control Systems Technology, IEEE Transactions on*, vol. 19, no. 4, pp. 832–842, July 2011.
- [15] Ariga Y., Pham H., Uemura M., Hirai H., and Miyazaki F., Novel equilibrium-point control of agonist-antagonist system with pneumatic artificial muscles. In *Robotics and Automation (ICRA), 2012 IEEE International Conference on*, pp. 1470–1475, May 2012.
- [16] Nakamura T., Tanaka D., and Maeda H., Joint stiffness and position control of an artificial muscle manipulator for instantaneous loads using a mechanical equilibrium model. *Advanced Robotics*, vol. 25, no. 3–4, pp. 387–406, 2011.